
Efficient Shapley Values for Attributing Global Properties of Diffusion Models to Data Groups

Chris Lin*, Mingyu Lu*, Chanwoo Kim Su-In Lee
Paul G. Allen School of Computer Science & Engineering
University of Washington
{clin25, mingyulu, suinlee}@cs.washington.edu

Abstract

As diffusion models are deployed in real-world settings, data attribution is needed to ensure fair acknowledgment for contributors of high-quality training data and to identify sources of harmful content. Previous work focuses on identifying individual training samples important for the generation of a given image. However, instead of focusing on a given generated image, some use cases require understanding global properties of the distribution learned by a diffusion model (e.g., demographic diversity). Furthermore, training data for diffusion models are often contributed in groups rather than separately (e.g., multiple artworks from the same artist). Hence, here we tackle the problem of attributing global properties of diffusion models to groups of training data. Specifically, we develop a method to efficiently estimate Shapley values by leveraging model pruning and fine-tuning. We empirically demonstrate the utility of our method with three use cases: (i) global image quality for a DDPM trained on a CIFAR dataset, (ii) demographic diversity for an LDM trained on CelebA-HQ, and (iii) overall aesthetic quality for a Stable Diffusion model LoRA-finetuned on Post-Impressionist artworks.

1 Introduction

Diffusion models have demonstrated impressive performance on image generation [22, 54], with models such as Dall-E 2 [45] and Stable Diffusion [47] showing versatile utilities and enabling downstream applications via customization [24, 48]. The training data for diffusion models are often scraped from the internet [51], raising concerns such as copyright attribution, harmful content generation [3], and bias propagation [40]. *Data attribution*, which aims to trace machine learning model behaviors back to training data, has the potential to address these issues. Indeed, in the context of supervised learning, data attribution methods have already been used to value data [14], identify adversarial samples [33], and discover similar data points [26].

Some recent work has developed data attribution methods for diffusion models [7, 13, 60, 63]. These methods focus on *local* properties related to the generation of a given image and aim to identify important *individual* training data. For example, Zheng et al. [63] showcase their method D-TRAK to study the changes in pixel values of particular generated images and find influential training samples. However, some use cases require understanding data’s influence on *global* model properties, which are related to the overall generative distribution of a diffusion model. For example, the demographic diversity of generated images can be considered a global property [40], and attributing this property to training data can help us identify potential sources of social biases in diffusion models. Furthermore, data for training diffusion models are often contributed *in groups* instead of separately, with each group corresponding to an entity of ownership (e.g., artworks by an artist; or images portraying a

*Equal contribution.

public figure). Therefore, here we address the problem of attributing *global* properties of diffusion models to *groups* of training data.

While diffusion models are increasingly monetized and groups of data can often correspond to copyright ownerships [50], attribution methods based on cooperative game theory are desirable because of their axiomatic justification. Particularly, the Shapley value provides a principled approach to fairly distribute monetary gains among contributors, since it is the unique notion that satisfies the four axioms for equitable valuation: *linearity*, *dummy player*, *symmetry*, and *efficiency* (see Section 3.1 for details) [14, 52]. Briefly, the Shapley value assesses each contributor based on the average gain incurred by adding the contributor to different contributor combinations. To estimate the Shapley values for data groups in our setting, we need to (i) retrain diffusion models on different subsets of groups; and (ii) measure global properties of the retrained models by running inference. However, training a diffusion model can take hundreds of GPU days, and inference can also be expensive (e.g., approximately 5 GPU days to generate 50,000 images for image quality metrics) [9]. Therefore, estimating Shapley values with vanilla retraining and inference is computationally impractical. Here, we propose to approximate retraining and retrained inference through model pruning and fine-tuning, thus enabling efficient Shapley value estimation (Figure 1).

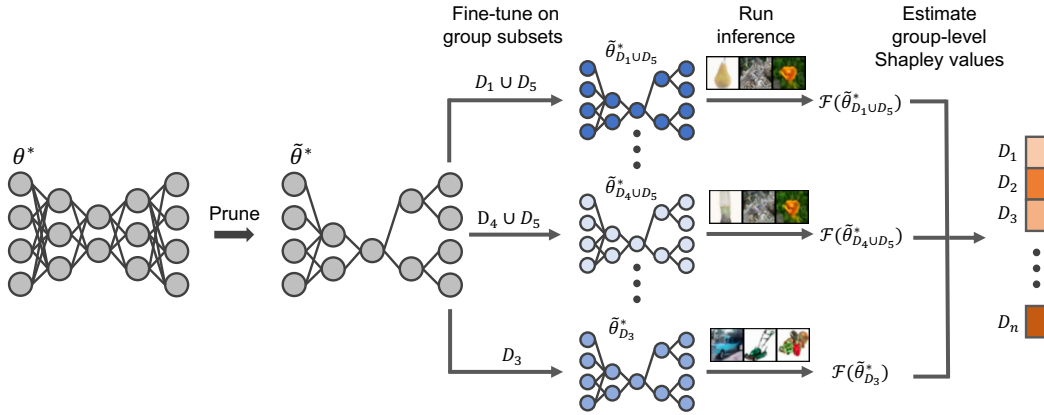


Figure 1: Schematic overview of our proposed method, where θ^* denotes a trained diffusion model that we aim to understand, and $\tilde{\theta}^*$ denotes the pruned model that approximates θ^* . After fine-tuning the pruned model on varying subsets of data groups, global model properties (\mathcal{F}) are measured on the fine-tuned models to estimate the Shapley value for each group of data.

Related work. The distinction between local and global model properties for supervised learning has been discussed in Covert et al. [6]. Here, this distinction is extended to generative models, where local properties correspond to a particular generated image, and global properties relate to the overall distribution learned by a generative model. The practical implications of group attribution have been discussed in the context of supervised learning [34].

Data attribution methods for diffusion models have been developed by recent work. Some methods require the models that we aim to understand be trained with specialized paradigms. For example, to assess the importance for a training sample, Dai and Gifford [7] first train an ensemble of diffusion models on data splits, followed by ablating models trained on splits containing the specific sample. Wang et al. [60] evaluate data attribution for text-to-image models by customizing a pretrained model toward an exemplar style. In contrast, other methods can be applied to already trained models. For example, the TRAK framework has been adapted to find important training data for intermediate latents along a generative process [13], while Zheng et al. [63] introduce empirical approaches that improve the performance of TRAK for diffusion models. All these methods attribute local model properties to individual data points, whereas our work focuses on attributing global model properties to data groups.

Contributions. (1) To our knowledge, we are the first to investigate how groups of training data influence global properties of diffusion models. (2) We propose a method that efficiently estimates group-level Shapley values for attributing global model properties, leveraging model pruning and

fine-tuning. (3) We empirically demonstrate that our method outperforms existing attribution methods across three datasets, model architectures, and global properties.

2 Preliminaries

This section provides an overview for diffusion models, global model property, group attribution, and existing attribution methods for diffusion models.

2.1 Diffusion Models

Our research primarily focuses on discrete-time diffusion models, specifically denoising diffusion probabilistic models (DDPMs) [22] and latent diffusion models (LDMs) [47]. Generally, diffusion models are trained to approximate a data distribution $q(\mathbf{x}_0)$. To perform learning, a training sample $\mathbf{x}_0 \sim q(\mathbf{x}_0)$ is sequentially corrupted by additive noise [22]. This procedure is called the *forward process* and is defined by $q(\mathbf{x}_t|\mathbf{x}_{t-1}) := \mathcal{N}(\mathbf{x}_t; \sqrt{1 - \beta_t}\mathbf{x}_{t-1}, \beta_t\mathbf{I})$, for $t = 1, \dots, T$, where $\{\beta_t\}_{t=1}^T$ corresponds to a variance schedule. Notably, the forward process allows sampling of \mathbf{x}_t at any time step t from \mathbf{x}_0 , with the closed form $q(\mathbf{x}_t|\mathbf{x}_0) = \mathcal{N}(\mathbf{x}_t; \sqrt{\bar{\alpha}_t}\mathbf{x}_0, (1 - \bar{\alpha}_t)\mathbf{I})$, where $\alpha_t := 1 - \beta_t$ and $\bar{\alpha}_t := \prod_{s=1}^t \alpha_s$. Then, a diffusion model learns to denoise $\mathbf{x}_{1:T}$, following the *reverse process* defined by $p_\theta(\mathbf{x}_{t-1}|\mathbf{x}_t) := \mathcal{N}(\mathbf{x}_{t-1}; \mu_\theta(\mathbf{x}_t, t), \sigma_t^2\mathbf{I})$, where $\theta \in \mathbb{R}^d$ is the model parameters, and σ_t corresponds to some sampling schedule [32]. Instead of modeling the conditional means μ_θ , it is standard to predict the added noises with a neural network ϵ_θ using the reparameterization trick. The training objective corresponds to a variational bound and is formulated as

$$\mathcal{L}_{\text{Simple}} = \mathbb{E}_{t,\epsilon} \left[\|\epsilon - \epsilon_\theta(\sqrt{\bar{\alpha}_t}x + \sqrt{(1 - \bar{\alpha}_t)}\epsilon, t)\|_2^2 \right] \quad (1)$$

Once a diffusion model has been trained, a new image can be generated by sampling an initial noise $\mathbf{x}_T \sim \mathcal{N}(\mathbf{0}, \mathbf{I})$ and iteratively applying ϵ_θ at each step $t = T, \dots, 1$ for denoising. In practice, the denoising process has various design choices, such as the number of inference time steps and output scaling [53, 54, 32]. Building upon diffusion models, LDMs [47] perform the stochastic process in the latent space of a pretrained encoder network. Additionally, it has been shown that one can condition diffusion models on additional information, such as a text prompt, allowing for explicit control over the semantics of the generated images through textual guidance [47].

2.2 Global Model Behavior

To gain a comprehensive understanding of machine learning models, it is often beneficial to study global model properties [6], which assess the model’s performance across samples, rather than focusing on individual outputs. For example, in the setting of supervised learning, global model property can be test accuracy. In the context of generative models, it can be a quality metric for generated samples. For example, in image generation, the global model property of interest can be the Inception Score [16] or FID [21]. More formally, a global model property for generative models is defined by any user-specified function $\mathcal{F} : \Theta \rightarrow \mathbb{R}$, which maps a generative model to a scalar value, thereby quantifying the overall distribution learned by the model.

Building on this, we introduce the problem of group attribution for global model properties. Similar to individual data attribution for local model properties [43, 63, 14], the goal of group attribution is to identify important groups of training data for a model’s global properties. Formally, we have the following definition.

Definition 1 Consider n groups of training samples $\mathcal{D} = \cup\{\mathcal{D}_i\}_{i=1}^n$ and a global model output function \mathcal{F} . A group attribution method is a function $\tau(\theta, \mathcal{F}, \{\mathcal{D}_i\}_{i=1}^n)$ that, given a model θ , assigns a score to each training group \mathcal{D}_i to indicate its importance to the global model output \mathcal{F} .

2.3 Attribution Methods for Diffusion Models

In the context of diffusion models, recent works have largely focused on local data attribution using TRAK [43], such as D-TRAK [63] and Journey-TRAK [13]. Generally, given a loss function \mathcal{L} and

models $\{\theta_s^*\}_{s=1}^S$ trained on S data subsets, TRAK is defined as below:

$$\frac{1}{S} \sum_{s=1}^S \phi^s(x)^\top \cdot \left(\Phi_{\text{TRAK}}^s \cdot \Phi_{\text{TRAK}}^s + \lambda I \right)^{-1} \Phi_{\text{TRAK}}^s \quad (2)$$

$$\Phi_{\text{TRAK}}^s = [\phi^s(x^1), \dots, \phi^s(x^n)]^\top, \text{ where } \phi^s(x) = \mathcal{P}_s^\top \nabla_\theta \mathcal{L}(x, \theta_s^*) \quad (3)$$

where \mathcal{P}_s is a random projection matrix. Building on this framework, Journey-TRAK [13] attributes training data not only for the final sample x but also for the noisy samples along the denoising process. Intriguingly, Zheng et al. [63] discover that replacing the loss function $\mathcal{L}_{\text{Simple}}$ with alternative functions results in superior performance.

While TRAK-based approaches for diffusion models are considered computationally efficient, they have several limitations. One key drawback is that their model property is confined to variants of the diffusion loss [63, 13], which can restrict their broader application. For example, some global model properties such as the distribution of cluster assignments [40] are not differentiable, making the gradient computations in TRAK infeasible. This highlights the need for developing another approach that can handle attribution for global model properties.

3 Group Attribution in Diffusion Models with the Shapley Value

In this section, we review the Shapley value and propose an efficient method to estimate Shapley values for diffusion models through model pruning and fine-tuning.

3.1 Shapley Attribution

The Shapley value was developed in cooperative game theory to fairly attribute credits in coalition games [52]. More formally in the context of group attribution, for training data with n groups, the Shapley value for a data group \mathcal{D}_i is defined as:

$$\beta_i := \frac{1}{n} \sum_{S \subseteq \mathcal{D} \setminus \{\mathcal{D}_i\}} \binom{n-1}{|S|}^{-1} (\mathcal{F}(\theta_{S \cup \{\mathcal{D}_i\}}) - \mathcal{F}(\theta_S)) \quad (4)$$

where S is a subset of training data groups $\{\mathcal{D}_1, \dots, \mathcal{D}_n\}$ and $\mathcal{F}(\theta_S)$ is the model property of a diffusion model trained on S . Shapley value assesses each group's contribution based on the weighted *marginal contribution*, $\mathcal{F}(\theta_{S \cup \{\mathcal{D}_i\}}) - \mathcal{F}(\theta_S)$. It satisfies axioms desirable for equitable attribution, including **linearity**, **dummy player**, **symmetry**, and **efficiency** [14]. There are arguments that the efficiency axiom, $\sum_{i=1}^n \beta_i = \mathcal{F}(\theta^*) - \mathcal{F}(\theta_\emptyset)$, where θ^* denotes the model trained on the entire dataset, may not always be essential in use cases where the primary goal is to remove detrimental data points [59]. In this setting, ranking is more important than exact importance values for removing such data points. However, in the context of generative models, particularly in applications involving monetary or credit allocation of some meaningful global model behavior measures, ensuring that the aggregate attribution of the data matches the total utility is crucial.

Despite its advantages, evaluating the Shapley value is challenging as it involves training 2^n (all possible subsets) models and computing their corresponding model behavior. Fortunately, many sampling-based estimators for Shapley values have been developed [41, 14, 56]. In particular, we can adopt KernelSHAP in the feature attribution literature for data attribution as an alternative by solving a weighted least squares problem with sampling [41, 5]:

$$\hat{\beta} = \min_{\beta_0, \dots, \beta_n} \frac{1}{M} \sum_{i=1}^M (\mathcal{F}(\theta_0) + \mathbf{1}_{S_i}^\top \beta - \mathcal{F}(\theta_{S_i}))^2 \quad \text{s.t.} \quad \mathbf{1}^\top \beta = \mathcal{F}(\theta^*) - \mathcal{F}(\theta_0) \quad (5)$$

where S_i is sampled following the distribution $\mu_{Sh}(S) \propto \frac{n-1}{\binom{n}{|S|} |S| (n-|S|)}$ for $1 < \mathbf{1}_{S_i}^\top \beta < n$; $\mathbf{1}_{S_i}$ is an indicator vector representing the presence of data group in S_i ; and θ_\emptyset is a randomly initialized model without training. By solving the least squares problem with the constraint via KKT conditions, a closed-form solution can be derived [5]. The obtained parameters $\hat{\beta}$ are the attribution scores.

3.2 Speed Retraining and Inference with Sparsified Fine-Tuning

While Equation (5) effectively reduces the number of diffusion models needed for Shapley value estimation, obtaining an adequate number of retrained models θ_{S_i} remains a challenge. The retraining time for models scales linearly with the number of sampled subsets, S_i , and the training duration for each diffusion model can be as large as hundred of GPU days [9]. To further decrease the computational burden needed to obtain θ_{S_i} , we propose a novel yet simple technique: **removal through sparsified fine-tuning** (Figure 1).

Specifically, our approach aims to approximate a model retrained with a subset S_i by fine-tuning the model θ^* on the subset S_i but with only a update steps. We also combine fine-tuning with model pruning using the *prune first, then unlearn* paradigm [29], leveraging model sparsity to make a more efficient approximation to retraining. We first perform pruning on θ^* and initially fine-tune it with \mathcal{D} to obtain a performant pruned model, $\tilde{\theta}^*$. Second, to obtain $\tilde{\theta}_{S_i}$, we apply fine-tuning [15, 57] on the subset S_i with the original diffusion loss, $\mathcal{L}_{\text{Simple}}$ [22].

$$\tilde{\theta}_{S_i} = \operatorname{argmin}_{\theta} \mathcal{L}(\tilde{\theta}^*, S_i) \quad \text{s.t.} \quad \mathcal{F}(\tilde{\theta}_{S_i}) \text{ (fine-tuning)} \approx \mathcal{F}(\theta_{S_i}) \text{ (retraining from scratch)} \quad (6)$$

By replacing θ_{S_i} with $\tilde{\theta}_{S_i}$ through the combined process of pruning and fine-tuning, we can drastically reduce the computational cost for obtaining $\tilde{\theta}_{S_i}$ and $\mathcal{F}(\tilde{\theta}_{S_i})$, expediting the removal-based attribution process of the Shapley value. In other words, under the same computational budget, compared to retaining, our proposed approach significantly increases the number of sampled S_i for estimating Eq. 5, thereby making the Shapley value feasible and practical for diffusion models.

4 Experiments

In this section, we compare our approach with existing attribution methods across various settings. We employ two primary metrics for evaluation: LDS and counterfactual analysis. Our findings demonstrate that our method significantly outperforms existing techniques in terms of efficacy.

4.1 Datasets

Datasets used for our experiments include CIFAR-20 (a subset of CIFAR-100), with 20 classes considered as groups for attribution; CelebA-HQ, with 50 celebrity identities considered as groups for attribution; and ArtBench (Post-Impressionism), with 258 artists considered as groups for attribution. More details about datasets can be found in Appendix A.

4.2 Setup for diffusion models

Model training. For CIFAR, we follow the original implementation of the unconditional DDPMs [22] where the model has 35.7M parameters (i.e., $d = 35.7 \times 10^6$ for $\theta \in \mathbf{R}^d$). For CelebA-HQ, we follow the implementation of LDM [47] with 274M parameters and a pre-trained VQ-VAE[46]. For both datasets, the maximum timestep is set to $T = 1000$ during training, with a linear variance schedule for the forward diffusion process ranging from $\beta_1 = 10^{-4}$ to $\beta_T = 0.02$. We use the Adam optimizer [39] and apply random horizontal flipping for data augmentation. Both the DDPM and LDM are trained for 20,000 steps with a batch size of 64 and a learning rate of 10^{-4} . During inference, images are generated using the 100-step DDIM solver [53]. For ArtBench (Post-Impressionism), the Stable Diffusion model [47] is fine-tuned using LoRA [24] with rank = 256, corresponding to 5.1M LoRA parameters. The prompt is set to "a Post-Impressionist painting" for each image. The model is trained using the AdamW optimizer [39] with a weight decay of 10^{-6} , for 200 epochs and a batch size of 64. Cosine learning rate annealing is used, with 500 warm-up steps and an initial learning rate of 3×10^{-4} . At inference time, images are generated using the PNDM scheduler with 100 steps [32].

Setup for pruning and fine-tuning. Magnitude-based pruning [19] is used remove model weights according to their magnitudes, resulting in sparse diffusion models with reduced parameters: from 35.7M to 19.8M for CIFAR-20 at a pruning ratio of 0.3, from 274M to 70.9M for CelebA-HQ at a ratio of 0.5, and from 5.1M to 2.6M for ArtBench (Post-Impressionism). To estimate Shapley values, the sparsified models are fine-tuned on subsets of data groups with 1,000 steps for CIFAR-20, 500 steps for CelebA-HQ, and 200 steps for ArtBench (Post-Impressionism).

Global model properties. For CIFAR-20, we aim to study which image classes contribute to overall image quality. Therefore, 10,240 samples are generated to compute the Inception Score (IS)²[49], defined as:

$$\text{IS} = \exp(\mathbb{E}_x[\text{KL}(p(y|x)||p(y))]) \quad (7)$$

where $p(y)$ represents the marginal class distribution over the generated data and $p(y|x)$ represents the conditional class distribution given a generated image x .

For CelebA-HQ, our goal is to investigate which celebrities contribute to demographic diversity. First, we generate 1,024 samples from the model trained using the full dataset. Following [40], we apply BLIP-VQA³[36] to extract image embeddings, which are then clustered into 20 distinct groups using the Ward linkage criterion [28], representing groups with demographic characteristics. Subsequently, for models trained on different subsets of celebrities, we also generate 1,024 samples, cluster them into those 20 clusters, and compute the entropy as a diversity measure:

$$\mathcal{H} = - \sum_{i=1}^n p_i \log(p_i) \quad (8)$$

where p_i is the proportion of samples in the i -th cluster.

For ArtBench (Post-Impressionism), we consider the use case where images are generated and the most aesthetically pleasing ones are kept. We simulate this use case by computing aesthetic scores⁴ for 50 generated images and considering the 90th percentile as the global model property.

4.3 Evaluating Group Attribution

Linear datamodeling score (LDS). From definition 1, for a given subset $S \subset \mathcal{D}$, we can define an additive model of global properties based on group attribution as follow:

$$g(S, \tau) := \sum_{i: \mathcal{D}_i \in S} \tau_i \quad (9)$$

Therefore, the evaluation for an attribution method τ can be constructed as follows:

Definition 2 (*Linear Datamodeling Score*) *Group attribution performance is measured using the linear datamodeling score (LDS) [26], which evaluates an attribution method by comparing linearly predicted model behaviors against actual retrained model behaviors. Let S_1, \dots, S_K be K randomly sampled subsets of the training set, each of size $\alpha \cdot n$ for some $\alpha \in (0, 1)$. The LDS for a group attribution score $\tau \in \mathbb{R}^n$ is defined as*

$$\text{LDS} := \rho(\{\mathcal{F}(\theta_{S_j})\}_{j=1}^K, \{g_\tau(S_j, \tau)\}_{j=1}^K), \text{ where } S_j \sim \text{Uniform}\{S \subset \mathcal{D} : |S| = \alpha \cdot n\}. \quad (10)$$

where ρ is the Spearman rank correlation [55], and θ_{S_j} denotes a model retrained from scratch with the group subset S_j .

We evaluate the LDS using 100 held-out subsets S_j , each sampled from the datamodel distribution with $\alpha = 0.25, 0.5, 0.75$ for each dataset, and calculate the corresponding global model behavior. We report the mean and the 95% confidence interval of the LDS scores across these experiments. We compared methods within three categories including similarity-based (baselines), TRAK-based (TRAKs), and our Shapley-based approach. More details about baseline methods⁵ can be found in Appendix C.1.

For TRAK-based methods and gradient similarity, we compute gradients and kernel2 using the final model checkpoint, meaning that $S = 1$ in Eq (2). In TRAK-based approaches, we select 100 timesteps evenly spaced within the interval $[1, T]$. For instance, for 100 timesteps, the selected timesteps are $\{1, 11, 21, \dots, 991\}$. At each timestep, we introduce one standard Gaussian noise. The projection dimensions are set at $k = 4096$ for CIFAR-20 and $k = 32768$ for CelebA and ArtBench. For D-TRAK, we adopt the best-performing model output function $\nabla_{\theta} \mathcal{L}_{\text{Square}}$ and choose $\lambda = 5e^{-1}$ as in [63].

²<https://github.com/sbarratt/inception-score-pytorch>

³<https://huggingface.co/Salesforce/blip-vqa-base>

⁴<https://github.com/LAIION-AI/aesthetic-predictor>

⁵TracIn is not considered because intermediate model checkpoints may not always be available in practice.

Counterfactual Evaluation. Following [63], we also apply the counterfactual evaluation [23]. We assess the change in model behavior, $\Delta\mathcal{F} = \frac{\mathcal{F}(\theta_k^*) - \mathcal{F}(\theta^*)}{\mathcal{F}(\theta^*)}$, by comparing the models trained before and after excluding the highest-ranked positive influential groups identified by different attribution methods. For this evaluation, we only choose the best-performing methods within baselines and TRAKs and perform top 40% removal. For CIFAR-20 and CelebA-HQ, models are retrained without the top influential groups with 10 random initializations. For ArtBench (Post-Impression), 5 models are retrained with different initializations.

4.4 Experiment Results

Shapley Attribution Outperforms TRAKs in Global Model Behavior

In Table 1, we present the LDS scores for baselines, TRAKs, and our method. Interestingly, similarity-based methods such as raw pixel, CLIP score, and gradient (without kernel) occasionally outperform TRAKs. We observe that TRAKs sometimes yield poor or even negative correlations when the model behavior \mathcal{F} is not directly linked to $\nabla_{\theta}\mathcal{L}$. Among TRAK-based approaches, attributing training samples using noisy latent (Journey-TRAK) during generation can result in an reverse attribution score in model behavior such as inception score and aesthetic score. Our findings suggest that when model behavior is not easily differentiable, using diffusion loss and its alternative functions, e.g. $\mathcal{L}_{\text{Square}}$, can lead to poor correlations and even result in reverse attribution.

On the other hand, our approach calculates group attributions using Shapley value with Equation (4) for each training sample, achieving the highest LDS scores of 61.48%, 26.34% , and 61.44% for CIFAR-20, CelebA-HQ, and ArtBench, respectively. This shows that attributing training samples based on their marginal contribution with respect to \mathcal{F} provides the most accurate importance score. For, CelebA-HQ, the overall lower LDS scores are expected due to the relatively small differences in the diversity score (entropy), suggesting that more instances may be needed to accurately compute Shapley values.

We compare the performance of attribution methods across varying subset sizes ($\alpha = 0.25, 0.5, 0.75$) in Appendix D. Although our approach consistently outperforms others, its performance decreases when the number of samples in S is small ($\alpha = 0.25$). This suggests that when training with very few data points (groups), the model may demonstrate different model behavior [30], or there could be non-linear interactions affecting attribution scores.

Table 1: LDS (%) results with $\alpha = 0.5$. Means and 95% confidence intervals across three random initializations are reported.

Method	CIFAR-20	CelebA-HQ	ArtBench (Post-Impressionism)
Pixel similarity (average)	-11.81 ± 4.56	-8.91 ± 0.93	11.24 ± 0.63
Pixel similarity (max)	-31.80 ± 2.90	21.70 ± 2.05	14.61 ± 2.72
Embedding dist. (average)	-	13.83 ± 1.12	-
Embedding dist. (max)	-	7.32 ± 3.16	-
CLIP similarity (average)	5.79 ± 3.67	-32.23 ± 0.87	-6.96 ± 4.08
CLIP similarity (max)	11.31 ± 0.37	-0.93 ± 3.83	-1.75 ± 4.07
Gradient similarity (average)	5.79 ± 3.67	25.93 ± 2.94	0.25 ± 1.18
Gradient similarity (max)	-0.89 ± 3.17	15.88 ± 5.98	10.48 ± 3.11
Aesthetic score (average)	-	-	24.85 ± 2.30
Aesthetic score (max)	-	-	21.36 ± 3.70
Relative IF	5.23 ± 5.50	12.65 ± 3.43	-5.02 ± 1.77
Renormalized IF	11.39 ± 6.79	9.22 ± 3.59	-11.41 ± 0.93
TRAK	7.94 ± 5.67	9.85 ± 3.62	-8.18 ± 1.30
Journey-TRAK	-42.92 ± 2.15	0.80 ± 4.98	-11.41 ± 4.22
D-TRAK	10.90 ± 1.21	-18.83 ± 2.12	11.30 ± 3.47
Sparsified-FT Shapley (Ours)	61.48 ± 2.27	26.34 ± 3.42	61.44 ± 2.04

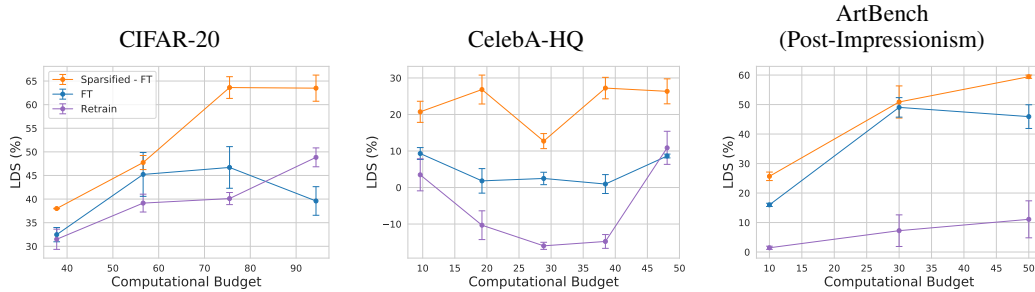


Figure 2: Comparison of LDS (%) with $\alpha = 0.5$ among Shapley values estimated with sparsified fine-tuning (FT), fine-tuning (FT), and retraining under the same computational budgets (1 unit = runtime to retrain and run inference on a full model).

Enhancing Fine-Tuning Efficiency Through Sparsification

Our sparsified fine-tuning approach significantly reduces the time required to compute θ_{S_i} compared to retraining, it is 5.3 and 10.4 times faster for CIFAR-20 and CelebA-HQ, respectively (Table 2). By enabling faster computation and obtaining more subset models, $\tilde{\theta}_{S_i}$, sparsified fine-tuning further enhances LDS. As shown in Figure 2, under the same computational budgets, sparsified fine-tuning yields the best LDS.

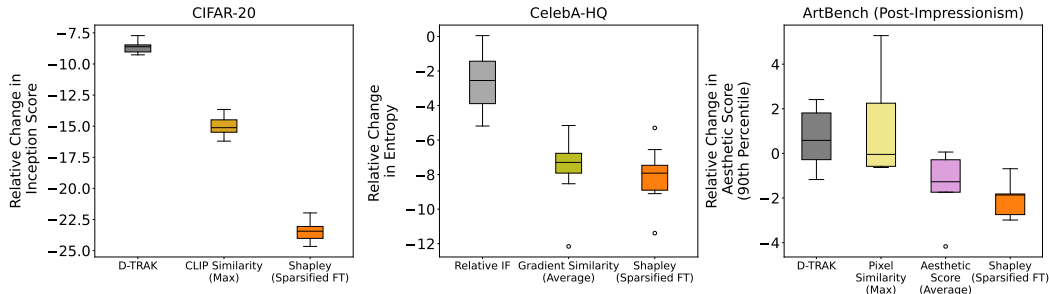


Figure 3: Relative percentage changes in global model properties, comparing the original fully trained models and models trained with the top 40% most important groups removed based on different attribution methods.

Counterfactual Evaluation

To further evaluate the attribution methods, we analyzed model behavior changes after removing the top influencers identified by each method. In the CIFAR-20 dataset, our approach showed changes of -23.44%, compared to -15.12% for CLIP similarity and -8.62% for D-TRAK, as shown in Figure 4 (Top). For CelebA-HQ, the changes were -7.92% for our method, -7.29% for gradient similarity, and +2.55% for relative IF. Additionally, we compared generated samples across retrained models for each method (Figure 4 and Figure 5). As shown in Figure 4, we visually note that for TRAK and CLIP score, automobiles are retrained, whereas our approach removes automobiles, suggesting that automobiles may have a significant impact on the Inception Score.

5 Discussion

In this work, we introduce the problem of attributing global model properties to groups of training data in the context of diffusion models. We develop an efficient method to estimate group-level Shapley values, leveraging model pruning and fine-tuning to speed up retraining and inference runtime compared to naive retraining. Empirical results across multiple datasets and global model properties demonstrate that our method outperforms existing attribution methods for diffusion models. There are several directions for future work. First, beyond fine-tuning, the field of machine unlearning

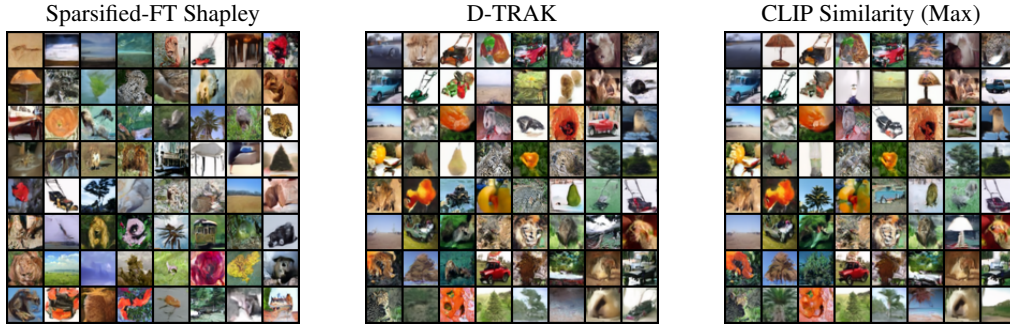


Figure 4: Images generated with the same initial noises for DDPMs trained without the top 40% most important CIFAR-20 classes based on sparsified-FT Shapley, D-TRAK, and CLIP similarity (max).

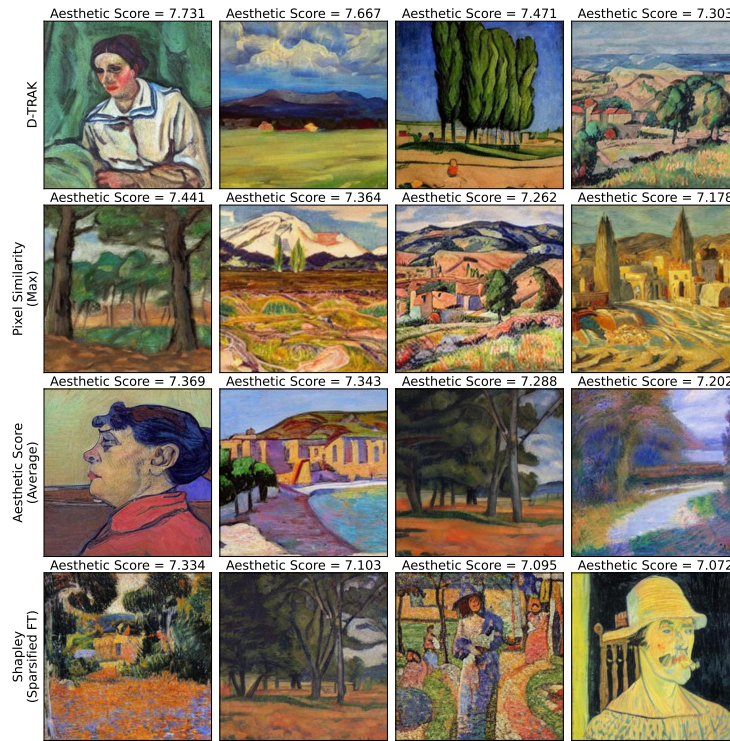


Figure 5: Two generated images above and two generated images below the 90th percentile of aesthetic scores, for Stable Diffusion models LoRA-finetuned without the top 40% most important artists based on D-TRAK, pixel similarity (max), training image aesthetic score (average), and sparsified-FT Shapley.

offers other methods such as gradient ascent and influence unlearning to approximate exact retraining [17, 27, 57]. There are also recent unlearning methods tailored for diffusion models [12, 20]. Exploring the design space of combining these methods with various pruning strategies [10, 11, 38] can be fruitful. Second, it can be useful to allocate group-level importance to individual data points within each group, providing two-level attributions. The Owen value, which modifies the Shapley value, is well suited for this scenario [42]. Finally, our method and existing attribution methods for diffusion models assume access to training data and model parameters, which are not necessarily available for deployed models. For vision-to-image models, membership inference and in-context learning may be useful in addressing this issue [25, 61].

References

- [1] Elnaz Barshan, Marc-Etienne Brunet, and Gintare Karolina Dziugaite. Relatif: Identifying explanatory training samples via relative influence. In *International Conference on Artificial Intelligence and Statistics*, pages 1899–1909. PMLR, 2020.
- [2] Samyadeep Basu, Philip Pope, and Soheil Feizi. Influence functions in deep learning are fragile. *arXiv preprint arXiv:2006.14651*, 2020.
- [3] Abeba Birhane, Vinay Uday Prabhu, and Emmanuel Kahembwe. Multimodal datasets: misogyny, pornography, and malignant stereotypes. *arXiv preprint arXiv:2110.01963*, 2021.
- [4] Guillaume Charpiat, Nicolas Girard, Loris Felardos, and Yuliya Tarabalka. Input similarity from the neural network perspective. *Advances in Neural Information Processing Systems*, 32, 2019.
- [5] Ian Covert and Su-In Lee. Improving KernelSHAP: Practical Shapley value estimation using linear regression. In *International Conference on Artificial Intelligence and Statistics*, pages 3457–3465. PMLR, 2021.
- [6] Ian Covert, Scott Lundberg, and Su-In Lee. Feature removal is a unifying principle for model explanation methods. *arXiv preprint arXiv:2011.03623*, 2020.
- [7] Zheng Dai and David K Gifford. Training data attribution for diffusion models. *arXiv preprint arXiv:2306.02174*, 2023.
- [8] Tim Dettmers, Mike Lewis, Sam Shleifer, and Luke Zettlemoyer. 8-bit optimizers via block-wise quantization. In *The Tenth International Conference on Learning Representations, ICLR 2022, Virtual Event, April 25-29, 2022*. OpenReview.net, 2022. URL <https://openreview.net/forum?id=shpkpVXzo3h>.
- [9] Prafulla Dhariwal and Alexander Nichol. Diffusion models beat gans on image synthesis. *Advances in neural information processing systems*, 34:8780–8794, 2021.
- [10] Xiaohan Ding, Guiguang Ding, Yuchen Guo, and Jungong Han. Centripetal sgd for pruning very deep convolutional networks with complicated structure. In *Proceedings of the IEEE/CVF conference on computer vision and pattern recognition*, pages 4943–4953, 2019.
- [11] Gongfan Fang, Xinyin Ma, and Xinchao Wang. Structural pruning for diffusion models. *Advances in neural information processing systems*, 36, 2024.
- [12] Rohit Gandikota, Joanna Materzynska, Jaden Fiotto-Kaufman, and David Bau. Erasing concepts from diffusion models. *arXiv preprint arXiv:2303.07345*, 2023.
- [13] Kristian Georgiev, Joshua Vendrow, Hadi Salman, Sung Min Park, and Aleksander Madry. The journey, not the destination: How data guides diffusion models. *arXiv preprint arXiv:2312.06205*, 2023.
- [14] Amirata Ghorbani and James Zou. Data shapley: Equitable valuation of data for machine learning. In *International conference on machine learning*, pages 2242–2251. PMLR, 2019.
- [15] Aditya Golatkar, Alessandro Achille, and Stefano Soatto. Eternal sunshine of the spotless net: Selective forgetting in deep networks. In *Proceedings of the IEEE/CVF Conference on Computer Vision and Pattern Recognition*, pages 9304–9312, 2020.
- [16] Ian J Goodfellow, Jonathon Shlens, and Christian Szegedy. Explaining and harnessing adversarial examples. *arXiv preprint arXiv:1412.6572*, 2014.
- [17] Laura Graves, Vineel Nagisetty, and Vijay Ganesh. Amnesiac machine learning. In *Proceedings of the AAAI Conference on Artificial Intelligence*, volume 35, pages 11516–11524, 2021.
- [18] Zayd Hammoudeh and Daniel Lowd. Identifying a training-set attack’s target using renormalized influence estimation. In *Proceedings of the 2022 ACM SIGSAC Conference on Computer and Communications Security*, pages 1367–1381, 2022.

- [19] Song Han, Jeff Pool, John Tran, and William Dally. Learning both weights and connections for efficient neural network. *Advances in neural information processing systems*, 28, 2015.
- [20] Alvin Heng and Harold Soh. Selective amnesia: A continual learning approach to forgetting in deep generative models. *arXiv preprint arXiv:2305.10120*, 2023.
- [21] Martin Heusel, Hubert Ramsauer, Thomas Unterthiner, Bernhard Nessler, and Sepp Hochreiter. Gans trained by a two time-scale update rule converge to a local nash equilibrium. *Advances in neural information processing systems*, 30, 2017.
- [22] Jonathan Ho, Ajay Jain, and Pieter Abbeel. Denoising diffusion probabilistic models. *Advances in neural information processing systems*, 33:6840–6851, 2020.
- [23] Sara Hooker, Dumitru Erhan, Pieter-Jan Kindermans, and Been Kim. A benchmark for interpretability methods in deep neural networks. *Advances in neural information processing systems*, 32, 2019.
- [24] Edward J Hu, Yelong Shen, Phillip Wallis, Zeyuan Allen-Zhu, Yuanzhi Li, Shean Wang, Lu Wang, and Weizhu Chen. Lora: Low-rank adaptation of large language models. *arXiv preprint arXiv:2106.09685*, 2021.
- [25] Hailong Hu and Jun Pang. Membership inference of diffusion models. *arXiv preprint arXiv:2301.09956*, 2023.
- [26] Andrew Ilyas, Sung Min Park, Logan Engstrom, Guillaume Leclerc, and Aleksander Madry. Datamodels: Predicting predictions from training data. *arXiv preprint arXiv:2202.00622*, 2022.
- [27] Zachary Izzo, Mary Anne Smart, Kamalika Chaudhuri, and James Zou. Approximate data deletion from machine learning models. In *International Conference on Artificial Intelligence and Statistics*, pages 2008–2016. PMLR, 2021.
- [28] Ward Jh Jr. Hierarchical grouping to optimize an objective function. *J. Amst. Statist. Assoc.*, 58: 236–244, 1963.
- [29] Jinghan Jia, Jiancheng Liu, Parikshit Ram, Yuguang Yao, Gaowen Liu, Yang Liu, Pranay Sharma, and Sijia Liu. Model sparsity can simplify machine unlearning. In *Annual Conference on Neural Information Processing Systems*, 2023.
- [30] Zahra Kadkhodaie, Florentin Guth, Eero P Simoncelli, and Stéphane Mallat. Generalization in diffusion models arises from geometry-adaptive harmonic representation. *arXiv preprint arXiv:2310.02557*, 2023.
- [31] Tero Karras, Timo Aila, Samuli Laine, and Jaakko Lehtinen. Progressive growing of gans for improved quality, stability, and variation. In *6th International Conference on Learning Representations, ICLR 2018, Vancouver, BC, Canada, April 30 - May 3, 2018, Conference Track Proceedings*. OpenReview.net, 2018. URL <https://openreview.net/forum?id=Hk99zCeAb>.
- [32] Tero Karras, Miika Aittala, Timo Aila, and Samuli Laine. Elucidating the design space of diffusion-based generative models. *Advances in Neural Information Processing Systems*, 35: 26565–26577, 2022.
- [33] Pang Wei Koh and Percy Liang. Understanding black-box predictions via influence functions. In *International conference on machine learning*, pages 1885–1894. PMLR, 2017.
- [34] Pang Wei W Koh, Kai-Siang Ang, Hubert Teo, and Percy S Liang. On the accuracy of influence functions for measuring group effects. *Advances in neural information processing systems*, 32, 2019.
- [35] Alex Krizhevsky, Geoffrey Hinton, et al. Learning multiple layers of features from tiny images. 2009.
- [36] Junnan Li, Dongxu Li, Caiming Xiong, and Steven Hoi. Blip: Bootstrapping language-image pre-training for unified vision-language understanding and generation. In *International conference on machine learning*, pages 12888–12900. PMLR, 2022.

- [37] Peiyuan Liao, Xiuyu Li, Xihui Liu, and Kurt Keutzer. The artbench dataset: Benchmarking generative models with artworks. *arXiv preprint arXiv:2206.11404*, 2022.
- [38] Liyang Liu, Shilong Zhang, Zhanghui Kuang, Aojun Zhou, Jing-Hao Xue, Xinjiang Wang, Yimin Chen, Wenming Yang, Qingmin Liao, and Wayne Zhang. Group fisher pruning for practical network compression. In *International Conference on Machine Learning*, pages 7021–7032. PMLR, 2021.
- [39] Ilya Loshchilov and Frank Hutter. Decoupled weight decay regularization. *arXiv preprint arXiv:1711.05101*, 2017.
- [40] Alexandra Sasha Luccioni, Christopher Akiki, Margaret Mitchell, and Yacine Jernite. Stable bias: Analyzing societal representations in diffusion models. *arXiv preprint arXiv:2303.11408*, 2023.
- [41] Scott M Lundberg and Su-In Lee. A unified approach to interpreting model predictions. In *Advances in Neural Information Processing Systems*, pages 4765–4774, 2017.
- [42] Guillermo Owen. Values of games with a priori unions. In *Mathematical economics and game theory: Essays in honor of Oskar Morgenstern*, pages 76–88. Springer, 1977.
- [43] Sung Min Park, Kristian Georgiev, Andrew Ilyas, Guillaume Leclerc, and Aleksander Madry. Trak: Attributing model behavior at scale. *arXiv preprint arXiv:2303.14186*, 2023.
- [44] Alec Radford, Jong Wook Kim, Chris Hallacy, Aditya Ramesh, Gabriel Goh, Sandhini Agarwal, Girish Sastry, Amanda Askell, Pamela Mishkin, Jack Clark, et al. Learning transferable visual models from natural language supervision. In *International conference on machine learning*, pages 8748–8763. PMLR, 2021.
- [45] Aditya Ramesh, Prafulla Dhariwal, Alex Nichol, Casey Chu, and Mark Chen. Hierarchical text-conditional image generation with clip latents. *arXiv preprint arXiv:2204.06125*, 1(2):3, 2022.
- [46] Ali Razavi, Aaron Van den Oord, and Oriol Vinyals. Generating diverse high-fidelity images with vq-vae-2. *Advances in neural information processing systems*, 32, 2019.
- [47] Robin Rombach, Andreas Blattmann, Dominik Lorenz, Patrick Esser, and Björn Ommer. High-resolution image synthesis with latent diffusion models. In *Proceedings of the IEEE/CVF conference on computer vision and pattern recognition*, pages 10684–10695, 2022.
- [48] Nataniel Ruiz, Yuanzhen Li, Varun Jampani, Yael Pritch, Michael Rubinstein, and Kfir Aberman. Dreambooth: Fine tuning text-to-image diffusion models for subject-driven generation. In *Proceedings of the IEEE/CVF Conference on Computer Vision and Pattern Recognition*, pages 22500–22510, 2023.
- [49] Tim Salimans, Ian Goodfellow, Wojciech Zaremba, Vicki Cheung, Alec Radford, and Xi Chen. Improved techniques for training gans. *Advances in neural information processing systems*, 29, 2016.
- [50] Pamela Samuelson. Generative ai meets copyright. *Science*, 381(6654):158–161, 2023.
- [51] Christoph Schuhmann, Romain Beaumont, Richard Vencu, Cade Gordon, Ross Wightman, Mehdi Cherti, Theo Coombes, Aarush Katta, Clayton Mullis, Mitchell Wortsman, et al. Laion-5b: An open large-scale dataset for training next generation image-text models. *Advances in Neural Information Processing Systems*, 35:25278–25294, 2022.
- [52] Lloyd S Shapley. A value for n-person games. *Contributions to the Theory of Games*, 2(28): 307–317, 1953.
- [53] Jiaming Song, Chenlin Meng, and Stefano Ermon. Denoising diffusion implicit models. *arXiv preprint arXiv:2010.02502*, 2020.
- [54] Yang Song, Jascha Sohl-Dickstein, Diederik P Kingma, Abhishek Kumar, Stefano Ermon, and Ben Poole. Score-based generative modeling through stochastic differential equations. *arXiv preprint arXiv:2011.13456*, 2020.

- [55] Charles Spearman. The proof and measurement of association between two things. 1961.
- [56] Erik Štrumbelj and Igor Kononenko. An efficient explanation of individual classifications using game theory. *Journal of Machine Learning Research*, 11:1–18, 2010.
- [57] Anvith Thudi, Gabriel Deza, Varun Chandrasekaran, and Nicolas Papernot. Unrolling sgd: Understanding factors influencing machine unlearning. In *2022 IEEE 7th European Symposium on Security and Privacy (EuroS&P)*, pages 303–319. IEEE, 2022.
- [58] Aäron van den Oord, Oriol Vinyals, and Koray Kavukcuoglu. Neural discrete representation learning. In Isabelle Guyon, Ulrike von Luxburg, Samy Bengio, Hanna M. Wallach, Rob Fergus, S. V. N. Vishwanathan, and Roman Garnett, editors, *Advances in Neural Information Processing Systems 30: Annual Conference on Neural Information Processing Systems 2017, December 4-9, 2017, Long Beach, CA, USA*, pages 6306–6315, 2017. URL <https://proceedings.neurips.cc/paper/2017/hash/7a98af17e63a0ac09ce2e96d03992fbc-Abstract.html>.
- [59] Jiachen T Wang and Ruoxi Jia. Data banzhaf: A robust data valuation framework for machine learning. In *International Conference on Artificial Intelligence and Statistics*, pages 6388–6421. PMLR, 2023.
- [60] Sheng-Yu Wang, Alexei A Efros, Jun-Yan Zhu, and Richard Zhang. Evaluating data attribution for text-to-image models. *arXiv preprint arXiv:2306.09345*, 2023.
- [61] Zhendong Wang, Yifan Jiang, Yadong Lu, Pengcheng He, Weizhu Chen, Zhangyang Wang, Mingyuan Zhou, et al. In-context learning unlocked for diffusion models. *Advances in Neural Information Processing Systems*, 36:8542–8562, 2023.
- [62] Chih-Kuan Yeh, Joon Kim, Ian En-Hsu Yen, and Pradeep K Ravikumar. Representer point selection for explaining deep neural networks. *Advances in neural information processing systems*, 31, 2018.
- [63] Xiaosen Zheng, Tianyu Pang, Chao Du, Jing Jiang, and Min Lin. Intriguing properties of data attribution on diffusion models. *arXiv preprint arXiv:2311.00500*, 2023.

Appendix

A Datasets

CIFAR (32 × 32). The CIFAR-100 dataset⁶[35] contains 50,000 training samples. To reduce computation, we also construct a CIFAR-20 dataset as a subset of CIFAR-100, which consists of 10,000 training samples randomly sampled from CIFAR-100’s training samples corresponding to the "large carnivores", "large omnivores and herbivores", "medium mammals", and "vehicles 1" classes.

CelebA-HQ (256 × 256). The original CelebA-HQ dataset [31] comprises 30,000 face images with 6,217 unique identities. We downloaded a preprocessed dataset with from <https://github.com/ndb796/LatentHSJA>, which contain 5,478 images from 307 identities, each with 15 or more images. For our experiment, we randomly sample 50 identities, totaling 895 images. Also, to match the input dimension required by the latent diffusion model implementation, we resize the original images from a resolution of 1024 × 1024 to 256 × 256.

ArtBench Post-Impressionism (256 × 256). ArtBench-10 is a dataset for benchmarking artwork generation with 10 art styles, consisting of 5,000 training images per style [37]. For our experiments, we consider the 5,000 training images corresponding to the art style "post-impressionism" from 258 artists.

B Additional Training Setup

For training diffusion models, we utilize NVIDIA GPUs: RTX 6000, A40, and A100, each equipped with 40GB, 40GB, and 24GB of memory respectively. This study employs the Diffusers library version 0.24.0⁷ to train various models across different datasets. Per-sample gradients are computed using the techniques outlined in the PyTorch library tutorial (version 2.2.1)⁸. Furthermore, we apply the TRAK library⁹ to project gradients with a random projection matrix, enhancing the efficiency of our computational methods. All experiments are conducted on systems equipped with 64 CPU cores and the specified NVIDIA GPUs.

For CelebA-HQ, we implement two techniques to reduce GPU memory usage during the training. First, we pre-compute the embedding of VQ-VAE module [58] for all training samples beforehand, since the VQ-VAE module is kept frozen during the training. This approach allows us to avoid loading the VQ-VAE module into GPU memory during training. Second, we use the 8-bit Adam optimizer implemented in bitsandbytes python package [8].

C Local Data Attribution

To compute local data attribution, several approaches have been proposed [1, 33, 14, 59, 26]. These methods can be broadly categorized into two types: 1) retraining-based approaches, which involve the removal and retraining of data points, and 2) influence function-based approaches, which calculate the impact of individual data points on the model’s predictions.

Influence function (IF), [33]. Influence function calculates the effect of infinitesimally up-weighting of a training sample $x^n \sim \mathcal{D}$ on the model output function $\mathcal{F}(x; \theta^*)$, measured on a sample of interest x by leveraging second-order approximation [33, 34, 2]. For a given model output \mathcal{F} , the data attribution score can be computed as

$$\tau_{IF}(x, \mathcal{D})_n = \nabla_{\theta} \mathcal{F}(x; \theta^*)^T \cdot \mathcal{H}_{\theta^*}^{-1} \cdot \nabla_{\theta} \mathcal{L}(x_n; \theta^*) \quad \text{for } n \in [N], \quad (11)$$

where $\mathcal{H}_{\theta^*} = \nabla_{\theta}^2 \mathcal{L}(D; \theta^*)$ is the Hessian matrix at the optimal parameters θ^* . Since influence-based approaches only require only the loss gradients computed at the sample to be explained and at the training samples [33, 62], it is sometimes more computationally efficient.

⁶<https://www.cs.toronto.edu/~kriz/cifar.html>

⁷<https://pypi.org/project/diffusers/>

⁸<https://pytorch.org/>

⁹<https://trak.csail.mit.edu/quickstart>

Removal by retraining. On the other hand, retraining-based approaches estimate the influence of a training sample x by removing x during the training procedure and assessing its marginal contribution [14, 59, 26]. The data attribution score is defined as

$$\tau_R(x, \mathcal{D})_n = \sum_{S \subseteq \mathcal{D} \setminus \{i\}} \mu(S) (\mathcal{F}(x; \theta_{S \cup \{i\}}) - \mathcal{F}(x; \theta_S)) \quad \text{for } n \in [N], \quad (12)$$

where S is a training data subset sampled from a distribution \mathcal{D} with training sample x_i removed and $\mu(S)$ are the corresponding distribution, such as Shapley or datamodel distribution [26, 14]. While retraining approaches have demonstrated superior performance, acquiring retraining models for subsets S is computationally expensive.

C.1 Data Attribution Methods for Diffusion Models

Here we provide definition and implementation details of the baselines used in Section 4. For TRAK-based approaches, we follow the implementation in ¹⁰.

Raw Pixel Similarity. This is a simple baseline that uses the raw image as the representation and then computes the cosine similarity between the sample of interest and each training sample as the attribution score. In particular, for both CelebA-HQ and ArtBench, we use the embeddings encoded by a pretrained model ^{11,12} of the raw images.

Embeddings Distance. This method computes the l_2 distances between training sample embeddings, generated using BLIP-VQA ¹³ [36], and the average embedding of training samples to determine similarity.

CLIP Similarity. This method utilizes CLIP ¹⁴ [44] to encode each sample into an embedding and compute the cosine similarity with each training sample as its attribution score.

Gradient. This is a gradient-based influence estimator [4] which computes the cosine similarity using the gradient representations of the sample and each training sample, as the attribution score

$$\begin{aligned} \tau(x, \mathcal{D})_n &= \mathcal{P}^\top \nabla_\theta \mathcal{L}_{\text{Simple}}(x; \theta^*)^\top \cdot \mathcal{P}^\top \nabla_\theta \mathcal{L}_{\text{Simple}}(x; \theta^*) \\ \tau(x, \mathcal{D})_n &= \frac{\mathcal{P}^\top \nabla_\theta \mathcal{L}_{\text{Simple}}(x; \theta^*)^\top \cdot \mathcal{P}^\top \nabla_\theta \mathcal{L}_{\text{Simple}}(x; \theta^*)}{\|\mathcal{P}^\top \nabla_\theta \mathcal{L}_{\text{Simple}}(x; \theta^*)^\top\| \|\mathcal{P}^\top \nabla_\theta \mathcal{L}_{\text{Simple}}(x; \theta^*)\|} \end{aligned} \quad (13)$$

TRAK. As discussed in Section 3, is defined as the following

$$\begin{aligned} \Phi_{\text{TRAK}}^s &= [\phi^s(x^1), \dots, \phi^s(x^n)]^\top, \text{ where } \phi^s(x) = \mathcal{P}_s^\top \nabla_\theta \mathcal{L}_{\text{Simple}}(x, \theta_s^*) \\ \tau_{\text{TRAK}}(x, \mathcal{D})_n &= \mathcal{P}_s^\top \nabla_\theta \mathcal{L}_{\text{Simple}}(x, \theta_s^*) \cdot \left(\Phi_{\text{TRAK}}^{s\top} \cdot \Phi_{\text{TRAK}}^s + \lambda I \right)^{-1} \mathcal{P}_s^\top \cdot \nabla_\theta \mathcal{L}_{\text{Simple}}(x^n, \theta_s^*) \end{aligned} \quad (14)$$

Relative Influence. Proposed by [1], the θ -relative influence functions estimator normalizes the [33] influence functions estimator by HVP magnitude. Following [63] we integrate this estimator with the TRAK methodology. The formulation is as follows:

$$\tau_{\text{TRAK}}(x, \mathcal{D})_n = \frac{\mathcal{P}^\top \nabla_\theta \mathcal{L}_{\text{Simple}}(x, \theta^*) \cdot \left(\Phi_{\text{TRAK}}^\top \cdot \Phi_{\text{TRAK}} + \lambda I \right)^{-1} \cdot \mathcal{P}^\top \nabla_\theta \mathcal{L}_{\text{Simple}}(x^n, \theta^*)}{\left\| \left(\Phi_{\text{TRAK}}^\top \cdot \Phi_{\text{TRAK}} + \lambda I \right)^{-1} \cdot \mathcal{P}^\top \nabla_\theta \mathcal{L}_{\text{Simple}}(x^n; \theta^*) \right\|} \quad (15)$$

Renormalized Influence. Introduced by [18], this method renormalizes the influence function by the magnitude of the training sample’s gradients. Similar to relative influence, we made an adoption following [63]. The method is calculated as follows:

$$\tau_{\text{TRAK}}(x, \mathcal{D})_n = \frac{\mathcal{P}^\top \nabla_\theta \mathcal{L}_{\text{Simple}}(x, \theta^*) \cdot \left(\Phi_{\text{TRAK}}^\top \cdot \Phi_{\text{TRAK}} + \lambda I \right)^{-1} \cdot \mathcal{P}^\top \nabla_\theta \mathcal{L}_{\text{Simple}}(x^n, \theta^*)}{\|\mathcal{P}^\top \nabla_\theta \mathcal{L}_{\text{Simple}}(x^n; \theta^*)\|} \quad (16)$$

¹⁰<https://github.com/sail-sg/D-TRAK/>

¹¹<https://github.com/CompVis/latent-diffusion/tree/main>

¹²<https://huggingface.co/lambdalabs/miniSD-diffusers>

¹³<https://huggingface.co/Salesforce/blip-vqa-base>

¹⁴<https://github.com/openai/CLIP>

Journey-TRAK. [13] focuses on attributing noisy images x_t . We follow [63] by averaging the attributions over the generation timesteps as follows

$$\tau_{\text{TRAK}}(x, \mathcal{D})_n = \frac{1}{T'} \sum_{t=1}^{T'} \mathcal{P}^\top \nabla_{\theta} \mathcal{L}_{\text{Simple}}(x_t, \theta^*) \cdot \left(\Phi_{\text{TRAK}}^\top \cdot \Phi_{\text{TRAK}} + \lambda I \right)^{-1} \cdot \mathcal{P}^\top \nabla_{\theta} \mathcal{L}_{\text{Simple}}(x^n, \theta^*) \quad (17)$$

TracIn [7, 60], which attributes the training sample’s influence to first-order approximation with saved checkpoints during the training process. However, this is also a major limitation because sometimes it’s impossible to obtain checkpoints for models such as Stable Diffusion [47].

D Additional Experiment Results

In this section, we provide additional experiment results.

Table 2: Average runtime in minutes (training + inference) for Shapley values estimated with retraining, fine-tuning (FT), and sparsified FT.

Method	CIFAR-20	CelebA-HQ	ArtBench (Post-Impressionism)
Retrain	77.4 + 20.8	213.4 + 26.5	190.6 + 6.4
FT	6.06 + 18.9	17.5 + 27.0	4.4 + 6.4
Sparsified FT	4.37 + 14.0	11.0 + 11.9	4.5 + 6.1

D.1 CIFAR-20

Table 3: LDS (%) results with $\alpha = 0.25, 0.5, 0.75$ on CIFAR-20, with the Inception Score of 10,240 generated images as the global model property. Means and 95% confidence intervals across three random initializations are reported.

Method	$\alpha = 0.25$	$\alpha = 0.5$	$\alpha = 0.75$
Pixel similarity (average)	-10.88 ± 9.61	-11.81 ± 4.56	-20.82 ± 5.57
Pixel similarity (max)	-17.42 ± 0.83	-31.80 ± 2.90	-23.88 ± 1.28
CLIP similarity (average)	-0.34 ± 4.65	-21.27 ± 1.37	-13.13 ± 1.96
CLIP similarity (max)	-1.19 ± 15.19	11.31 ± 0.37	16.05 ± 7.30
Gradient similarity (average)	6.48 ± 10.98	5.79 ± 3.67	-10.75 ± 7.06
Gradient similarity (max)	7.22 ± 3.88	-0.89 ± 3.17	-4.82 ± 4.71
Relative IF	1.14 ± 13.51	5.23 ± 5.50	5.21 ± 3.78
Renormalized IF	9.09 ± 13.40	11.39 ± 6.79	7.99 ± 4.02
TRAK	3.62 ± 14.02	7.94 ± 5.67	6.59 ± 3.88
Journey-TRAK	-30.09 ± 3.85	-42.92 ± 2.15	-40.43 ± 3.46
D-TRAK	21.02 ± 6.76	10.90 ± 1.21	21.90 ± 5.02
Sparsified-FT Shapley (Ours)	51.24 ± 3.39	61.48 ± 2.27	59.15 ± 4.24

Table 4: LDS (%) results on Removal-Based Methods with different number of subset S .

α	Method	$S = 100$	$S = 200$	$S = 300$	$S = 400$	$S = 500$
0.25	Retraining	43.88 (3.97)	49.95 (3.20)	57.56 (2.52)	62.68 (1.85)	65.90 (1.52)
	Sparsified-FT	8.46 (13.41)	23.92 (6.27)	33.88 (8.33)	54.88 (7.44)	51.24 (3.39)
	FT	13.57 (7.09)	40.01 (8.30)	28.94 (8.59)	24.58 (6.07)	20.57 (3.02)
0.5	Retraining	48.84 (2.00)	39.55 (3.17)	57.24 (2.69)	66.81 (2.99)	70.58 (2.05)
	Sparsified-FT	-5.41 (4.78)	38.00 (3.06)	47.74 (1.49)	63.62 (2.30)	61.48 (2.27)
	FT	13.57 (7.09)	40.01 (8.30)	28.94 (8.59)	24.58 (6.07)	20.57 (3.02)
0.75	Retraining	51.39 (3.21)	45.85 (3.99)	61.91 (4.62)	70.59 (3.13)	72.07 (4.83)
	Sparsified-FT	-11.44 (2.26)	33.98 (0.98)	48.16 (5.18)	59.65 (5.34)	59.15 (4.24)
	FT	33.90 (5.88)	26.09 (8.55)	45.49 (6.83)	46.92 (5.96)	38.51 (4.62)

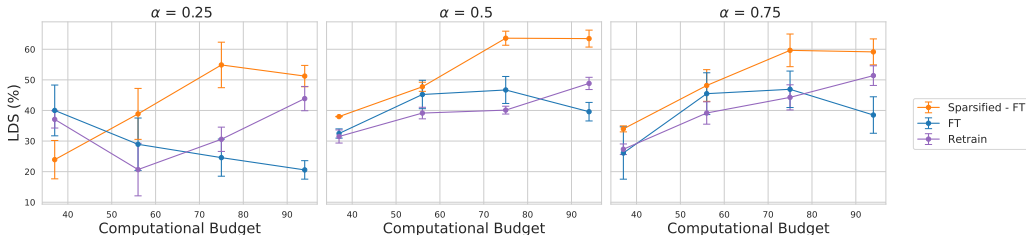


Figure 6: LDS (%) results on CIFAR-20 for Shapley values estimated with sparsified fine-tuning (FT), finet-tuning (FT), and retraining under the same computational budgets (1 unit = runtime to retrain and run inference on a full model).



Figure 7: Inception scores and example images generated with the same initial noises for DDPMs trained without the 10%, 20%, and 40% (top to bottom) most important CIFAR-20 classes based on sparsified-FT Shapley, D-TRAK, and CLIP similarity (max).

D.2 CelebA-HQ

Table 5: LDS (%) results with $\alpha = 0.25, 0.5, 0.75$ on CelebA-HQ, with the cluster entropy of 1,024 generated images as the global model property. Means and 95% confidence intervals across three random initializations are reported.

Method	$\alpha = 0.25$	$\alpha = 0.5$	$\alpha = 0.75$
Pixel similarity (average)	-1.52 ± 3.14	-8.91 ± 0.93	-4.19 ± 2.25
Pixel similarity (max)	9.53 ± 6.35	21.70 ± 2.05	24.76 ± 0.96
Embedding dist. (average)	3.59 ± 6.47	13.83 ± 1.12	10.89 ± 2.04
Embedding dist. (max)	9.17 ± 2.12	7.32 ± 3.16	22.25 ± 1.87
CLIP similarity (average)	-8.29 ± 4.38	-32.23 ± 0.87	-22.29 ± 2.56
CLIP similarity (max)	-23.62 ± 3.51	-0.93 ± 3.83	-8.86 ± 2.16
Gradient similarity (average)	28.04 ± 3.57	25.93 ± 2.94	29.23 ± 0.96
Gradient similarity (max)	9.61 ± 1.17	11.15 ± 5.90	18.70 ± 1.66
Relative IF	19.07 ± 4.08	12.62 ± 3.43	13.72 ± 1.90
Renormalized IF	13.33 ± 3.33	9.22 ± 3.59	9.57 ± 1.92
TRAK	16.73 ± 3.73	9.85 ± 3.62	10.50 ± 1.79
Journey-TRAK	7.34 ± 0.27	-8.00 ± 4.98	-7.80 ± 1.53
D-TRAK	-6.89 ± 6.01	-18.83 ± 2.12	-18.54 ± 0.78
Sparsified-FT Shapley (Ours)	10.05 ± 5.33	26.34 ± 3.34	24.08 ± 1.52

Table 6: LDS (%) results on Removal-Based Methods with different number of subsets S

α	Method	$S = 100$	$S = 200$	$S = 300$	$S = 400$	$S = 500$
0.25	Retraining	3.54 (0.59)	8.91 (2.61)	16.77 (4.75)	15.58 (6.23)	31.52 (5.56)
	Sparsified - FT	9.95 (5.77)	15.93 (6.29)	9.90 (8.17)	16.12 (6.40)	10.05 (5.33)
	FT (500 steps)	-10.52 (4.26)	2.77 (5.79)	12.29 (4.50)	9.86 (4.84)	13.91 (3.91)
0.5	Retraining	19.01 (1.60)	28.43 (2.71)	35.06 (3.48)	23.48 (2.95)	28.58 (3.91)
	Sparsified - FT	20.73 (2.89)	26.83 (3.96)	12.71 (2.06)	27.23 (2.94)	26.34 (3.42)
	FT (500 steps)	1.82 (3.36)	9.25 (2.59)	12.17 (2.83)	8.63 (0.52)	13.77 (1.42)
0.75	Retraining	21.14 (0.93)	26.29 (1.37)	31.87 (2.85)	31.60 (2.23)	32.26 (2.08)
	Sparsified - FT	16.05 (0.31)	29.35 (1.43)	9.49 (2.03)	17.70 (1.30)	24.08 (1.52)
	FT (500 steps)	-11.02 (1.51)	-12.07 (4.30)	1.93 (4.82)	0.96 (4.16)	7.37 (3.79)

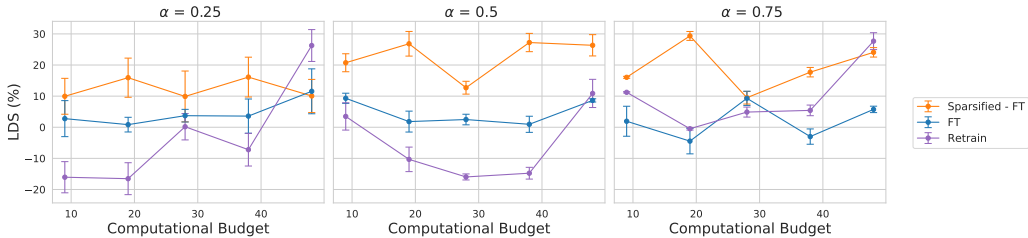


Figure 8: LDS (%) results on CelebA-HQ for Shapley values estimated with sparsified fine-tuning (FT), fine-tuning (FT), and retraining under the same computational budgets (1 unit = runtime to retrain and run inference on a full model).

D.3 ArtBench (Post-Impressionism)

Table 7: LDS (%) results with $\alpha = 0.25, 0.5, 0.75$ on ArtBench (Post-Impressionism), with the 90th percentile of aesthetic scores for 50 generated images as the global model property. Means and 95% confidence intervals across three random initializations are reported.

Method	$\alpha = 0.25$	$\alpha = 0.5$	$\alpha = 0.75$
Pixel similarity (average)	16.57 (3.16)	11.24 (0.63)	-1.19 (5.71)
Pixel similarity (max)	16.62 (2.95)	14.61 (2.72)	3.43 (10.57)
CLIP similarity (average)	-6.03 (1.61)	-6.96 (4.08)	-9.27 (2.74)
CLIP similarity (max)	8.94 (0.43)	-1.75 (4.07)	-1.70 (9.89)
Grad similarity (average)	4.14 (5.14)	0.25 (1.18)	-7.81 (0.89)
Grad similarity (max)	22.10 (9.02)	10.48 (3.11)	1.32 (4.19)
Aesthetic score (average)	24.81 (3.00)	24.85 (2.30)	13.21 (7.82)
Aesthetic score (max)	31.73 (3.04)	21.36 (3.70)	7.45 (11.66)
Relative IF	3.30 (4.98)	-5.02 (1.77)	-3.77 (12.05)
Renormalized IF	-1.71 (4.37)	-11.41 (0.93)	-8.96 (12.86)
TRAK	-0.85 (4.74)	-8.18 (1.30)	-6.78 (13.37)
Journey-TRAK	-14.10 (5.09)	-11.41 (4.22)	-6.83 (2.80)
D-TRAK	19.37 (3.29)	11.30 (3.47)	17.72 (6.87)
Sparsified-FT Shapley (Ours)	52.83 (3.58)	61.44 (2.04)	32.24 (10.93)

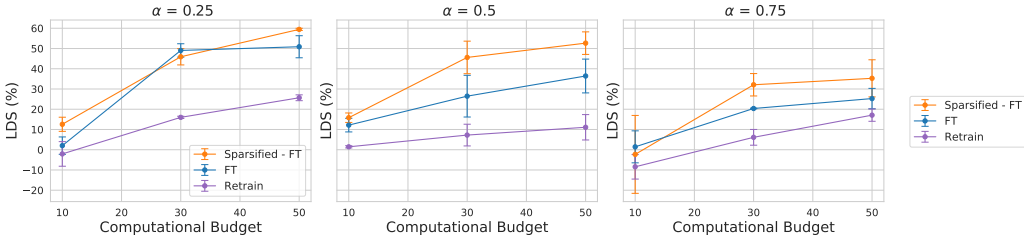


Figure 9: LDS (%) results with $\alpha = 0.25, 0.5, 0.75$ on ArtBench (Post-Impressionism) for Shapley values estimated with sparsified fine-tuning (FT), fine-tuning (FT), and retraining under the same computational budgets (1 unit = runtime to retrain and run inference on a full model).

Table 8: Aesthetic Score (90th percentile of 50 generated images) as the global model behavior. 100 datamodel subsets with alpha = 0.25, 0.5, 0.75 are used for evaluation. Means and 95% confidence intervals across three random initializations are reported. All Shapley values are estimated with 1,000 subsets.

α	Retrain	Sparsified - FT	FT
0.25	53.25 (6.75)	51.15 (7.54)	52.83 (3.58)
0.50	52.30 (2.32)	51.61 (3.21)	61.44 (2.04)
0.75	23.78 (14.07)	33.77 (6.65)	32.24 (10.93)



Figure 10: Two generated images above and two generated images below the 90th percentile of aesthetic scores, for Stable Diffusion models LoRA-finetuned without the top 40% most important artists based on D-TRAK, pixel similarity (max), training image aesthetic score (average), and sparsified-FT Shapley.



Figure 11: Two generated images above and two generated images below the 90th percentile of aesthetic scores, for Stable Diffusion models LoRA-finetuned without the top 40% most important artists based on D-TRAK, pixel similarity (max), training image aesthetic score (average), and sparsified-FT Shapley.

E Broader Impact

In our work, we introduce the problem of attributing global model properties to groups of training data in the context of diffusion models. As the broader application of generative models, it's crucial to correctly attribute training data. To address this, we develop a novel methodology that not only enhances understanding of how data influences model behavior but also improves the transparency of generative models. By systematically analyzing the impact of different data subsets, our approach facilitates more informed modifications to the training process, ultimately leading to more robust and reliable generative models. This capability is essential for deploying these models in real-world scenarios where accuracy and accountability are paramount.